



1 **Quantifying large methane emissions from the Nord Stream**
2 **pipeline gas leak of September 2022 using IASI satellite**
3 **observations and inverse modelling**

4
5 Chris Wilson^{1,2}, Brian J. Kerridge^{3,4}, Richard Siddans^{3,4}, David P. Moore^{5,6}, Lucy J.
6 Ventress^{3,4}, Emily Dowd², Wuhu Feng^{2,7}, Martyn P. Chipperfield^{1,2}, John J. Remedios^{5,6}

7
8 ¹National Centre for Earth Observation, University of Leeds, Leeds, UK.

9 ²School of Earth & Environment, University of Leeds, Leeds, UK.

10 ³National Centre for Earth Observation, STFC Rutherford Appleton Laboratory, Chilton, UK.

11 ⁴Remote Sensing Group, STFC Rutherford Appleton Laboratory, Chilton, UK.

12 ⁵National Centre for Earth Observation, University of Leicester, Leicester, UK.

13 ⁶School of Physics and Astronomy, University of Leicester, Leicester, UK.

14 ⁷National Centre for Atmospheric Science, University of Leeds, Leeds, UK.

15
16 *Correspondence to:* Chris Wilson (c.wilson@leeds.ac.uk)

17
18 **Abstract**

19
20 The sudden leaks from the Nord Stream gas pipelines, which began in September 2022, released a substantial
21 amount of methane (CH₄) into the atmosphere. From the IASI instrument onboard EUMETSAT's MetOp-B, we
22 document the first satellite-based retrievals of column-average CH₄ (XCH₄) that clearly show the large CH₄
23 plume emitted from the pipelines. The data displays elevations greater than 200 parts per billion (ppb, ~11%)
24 above observed background values (1882 ± 21 ppb). Based on the IASI data, together with an integrated mass
25 enhancement technique and formal model-based inversions applied for the first time to thermal infrared satellite
26 methane plume data, we quantify the total mass of CH₄ emitted to the atmosphere during the first two days of
27 the leaks to be 215 - 390 Gg CH₄. Substantial temporal heterogeneity is displayed in our model-derived flux
28 rate, with three distinct peaks in emission rate over the first two days. Our range overlaps with other previous
29 estimates, which were 75 – 230 Gg CH₄ and were mostly based on inversions that assimilated *in situ*
30 observations from nearby tower sites. However, our derived values are generally larger than those previous
31 results, with the differences likely due to the fact that our results are the first to use satellite-based observations
32 of XCH₄ from the days following the leaks. We incorporate multiple satellite overpasses that monitored the CH₄
33 plume as it was transported across Scandinavia and the North Sea up to the evening of the 28th September 2022.
34 We produced model simulations of the atmospheric transport of the plume using the Eulerian atmospheric
35 transport model, TOMCAT, which show good representation of the plume location in the days following the
36 leaks. The simulated CH₄ mixing ratios at three of the four nearby *in situ* measurement sites are larger than the
37 observed *in situ* values by up to hundreds of ppb, which highlights the challenges inherent in representing short-
38 term plume movement over a specific location using a model such as TOMCAT with a relatively coarse
39 Eulerian grid. Our results confirm the leak of the Nord Stream pipes to clearly be the largest individual fossil
40 fuel-related leak of CH₄ on record, greatly surpassing the previous largest leak (95 Gg CH₄) at the Aliso Canyon
41 gas facility in California in 2015-16.

42



43 **1. Introduction**

44
45 Nord Stream is an offshore submerged pipeline network which carries natural gas from Russian facilities into
46 Western Europe. The network is made up of two pipelines (NS1 and NS2), each originating in Russia and
47 running through the Baltic Sea to Lubmin, Germany (Figure 1). NS1 has been operating since 2011 but the NS2
48 pipeline has not yet entered service, although it has carried natural gas. On 26th September 2022, multiple
49 significant underwater gas leaks from these pipelines were detected by Nord Stream and the Danish Energy
50 Agency, with apparently substantial gas emission through the water to the atmosphere (Danish Energy Agency,
51 2022). This was monitored by multiple national and international bodies over the following days. NS2 first
52 began to leak on the morning of 26th September, from a location (15.41°E, 54.88°N) near the Danish island of
53 Bornholm, whilst leaks were detected from NS1 at two more northerly locations (15.60°E, 55.54°N and
54 15.79°E, 55.56°N) later that day (Figure 1). There were reports of explosions in the area around the times that
55 these leaks were detected (e.g. GEUS, 2022), and the pressure in the pipelines underwent an abrupt and
56 dramatic decrease, indicative of sudden ruptures in the pipes. Neither pipeline was transporting natural gas into
57 Europe at the time, but both contained substantial quantities of gas, the vast majority of which is methane (CH₄).
58 This was released to the water and detected as large bubbles at the surface as it was further emitted into the
59 atmosphere. Regions up to 0.7 km in diameter of rising gas bubbles were detected at the surface by *in situ*
60 monitoring teams and by various satellite high-resolution imagers (e.g. Jia et al., 2022). The release of gas from
61 the pipelines continued for a number of days before the Danish Energy Agency declared that the leaks had
62 ceased on October 2nd 2022.

63 CH₄ is the second most significant greenhouse gas after carbon dioxide (CO₂). Human-induced emissions of
64 CH₄ have been responsible for 1.19 [0.81 – 1.58] Wm⁻² of anthropogenic effective radiative forcing since 1750
65 (net total of 2.72 [1.96 – 3.48] W m⁻², Szopa et al. (2021)), with recent international agreements (UNFCCC,
66 2015; European Commission, 2021) having been put in place to urgently and significantly reduce CH₄
67 emissions for many countries. Recent satellite observations have shown that there are hundreds of CH₄ point
68 source leaks worldwide contributing to direct anthropogenic emissions (e.g. Lauvaux et al., 2022). Growing
69 levels of atmospheric CH₄ also adversely affect human health by contributing to increasing tropospheric ozone
70 (West et al., 2006). A sudden large release of CH₄ into the atmosphere such as the one from Nord Stream could
71 have significant consequences in terms of climate change and health. It is therefore important that the CH₄
72 emitted to the atmosphere during the Nord Stream leaks is accurately quantified. Various estimates, ranging
73 from 75 to 230 Gg CH₄ (75,000 – 230,000 tonnes), have been suggested as to the quantity of CH₄ released to the
74 atmosphere through assorted methodologies (see Jia et al. (2022); UNEP & IMEO (2023)).

75 Previous observational and modelling work (NILU, 2022; CAMS, 2022; NCEO, 2022; Jia et al., 2022) has
76 shown that a plume of CH₄ originating from the location leaks was initially transported eastwards towards
77 Finland's southern coast on 26th and 27th September, before a change in the wind direction then pushed it back
78 out across Sweden and Norway and out into the North Sea to the north of Scotland late on the 27th and 28th.
79 Significantly elevated near-surface CH₄ concentrations were briefly observed at a number of Integrated Carbon
80 Observation System (ICOS) measurement towers in Scandinavia over the course of these three days, but there
81 has been no direct satellite retrieval of downwind CH₄ concentrations available for the area to provide a more
82 complete observation of the plume.



83 The Infrared Atmospheric Sounding Interferometer (IASI), on board EUMETSAT's MetOp-B satellite, is an
84 across-track scanning thermal infrared sounder from which CH₄ distributions can be retrieved twice per day
85 with high accuracy (Siddans et al., 2017). IASI's regular overpass times meant that it observed the area
86 surrounding the CH₄ leak at approximately 09:30 and 21:30 local time each day. Thanks to favourable
87 observing conditions, IASI observed enhanced CH₄ concentrations over the Baltic and the North Sea in the days
88 following the detection of the Nord Stream leaks. We use this data, together with *in situ* observations from the
89 ICOS network and an atmospheric chemical transport model, in order to quantify the total CH₄ emitted to the
90 atmosphere from Nord Stream during the first two days of the leaks. This is the first time that plume flux
91 inversions have been carried out using thermal infrared satellite data. Here we describe the results of this
92 quantification and put into context the derived CH₄ contribution from these leaks compared both with previous
93 similar large gas releases and with the global CH₄ budget.

94 Section 2 describes the IASI methane retrieval scheme used in this study, the CH₄ distributions retrieved from
95 the satellite and the ICOS data. Section 3 describes the atmospheric model and the inverse modelling technique.
96 We present our results in Section 4, before discussing their implications and concluding our discussion in
97 Sections 5 and 6, respectively.

98
99

100 2. Observations

101

102 2.1 IASI retrievals

103

104 IASI is a cross-track-scanning Michelson interferometer (Blumstein et al., 2004) housed onboard the
105 EUMETSAT polar-orbiting MetOp-B satellite, which was launched in 2012. Identical instruments are hosted on
106 MetOp-A and -C, launched in 2006 and 2018, respectively, although MetOp-A is no longer operational. IASI
107 provides daily global coverage with four circular footprints of approximately 12 km diameter at nadir, arranged
108 in a 2 × 2 square grid of size 50 × 50 km. The IASI instrument measures upwelling thermal infrared radiation
109 (TIR) with 8461 channels at 0.25 cm⁻¹ spectral resolution, ranging from 645 to 2760 cm⁻¹. Observations are
110 made at approximately 09:30 (descending node) and 21:30 (ascending node) local time each day. Column-
111 average CH₄ distributions used here were retrieved using an updated version (v2.0) of a scheme developed
112 originally for MetOp-A (Siddans et al., 2017), which has since been applied to MetOp-B (Knappett et al., 2022)
113 and running in near-real time at the Rutherford Appleton Laboratory (RAL) in Oxfordshire, UK
114 (<http://rsg.rl.ac.uk/vistool>). Updates included in the v2.0 scheme include improved representation of prior
115 covariance, changes to spectroscopy in the radiative transport model, an updated elevation model and
116 improvements to the representation of cloud, temperature and emissivity (Buchwitz et al., 2023). The v2.0
117 scheme retrieves CH₄ from measurements of its spectral signature in the 7.9 μm (1,260 cm⁻¹) region (ν₄
118 fundamental vibration-rotation band). Vertical sensitivity generally peaks in the mid-upper troposphere since the
119 spectral absorption signature is determined by temperature contrast with the surface. These data have previously
120 been used for various studies of the atmosphere (e.g. Robson et al. (2020); Pope et al. (2021); Pimlott et al.
121 (2022); Buchwitz et al. (2023)).

122



123 Elevated CH₄ mixing ratios were observed by IASI in the Baltic Sea above the leak sites on the morning of 26th
124 September (Figure 2). However, cloudy conditions over much of Scandinavia and the North Sea meant that the
125 plume was not detected during the evening overpass on 26th September nor on the morning of 27th September.
126 Very high CH₄ concentrations were then detected over the North Sea off the west coast of Norway on the
127 evening of September 27th and morning and evening of September 28th. On the morning of September 28th, in
128 particular, a very distinct plume shape was detectable in IASI data, with areas of enhanced CH₄ around the
129 northern and southern regions of the Norwegian coast. After that day, the plume became too diffuse to be
130 distinguished from background concentrations. Retrieved column-averaged CH₄ (XCH₄) enhancements within
131 the plume on the morning of the 28th are up to 200 ppb (~11%), relative to the nearby background CH₄ mixing
132 ratios of 1882 ± 21 ppb (mean and standard deviation). The IASI retrievals documented here are the only
133 satellite observations of the Baltic Sea, Scandinavia and North Sea regions that captured a coherent XCH₄
134 plume from the Nord Stream leaks in the days immediately after the leaks began. On 30th September 2022, the
135 GHGSat group's satellite constellation did capture a plume as it was emitted immediately above the leak
136 location (GHGSat, 2022), although this was some days after the leaks began and by this point the emission rate
137 was fairly small (~0.08 Gg hr⁻¹). Although they operate at very high spatial resolution, GHGSat satellites
138 retrieve only the CH₄ enhancement above the background, rather than total XCH₄, and only targets specific
139 sources. Meanwhile, Landsat-8-OLI and Sentinel-2B also detected enhanced CH₄ from high resolution images
140 over the leak locations on 29th and 30th September (Jia et al., 2022), although these retrievals had large
141 uncertainties associated with them.

142

143 2.2 ICOS network

144

145 Consistent *in situ* monitoring of CH₄ mixing ratios is carried out by the Integrated Carbon Observation System
146 (ICOS) network (Levin et al., 2020; Heiskanen et al., 2022, <https://www.icos-cp.eu/>), a group of more than 140
147 tall tower monitoring stations located across Europe and Great Britain, including a number of measurement sites
148 around southern Scandinavia. These sites measure greenhouse gas mixing ratios and fluxes in the atmosphere,
149 ecosystems and oceans. There are four sites near Scandinavia that continuously measure CO₂, CH₄ and carbon
150 monoxide (CO) mixing ratios at multiple heights between 10 m and 150 m above the surface. These are located
151 at Birkenes, Norway (BIR, 8.3°E, 58.4°N, 219 metres above sea level (masl)); Hyltemossa, Sweden (HTM,
152 13.4°E, 56.1°N, 115 masl); Norunda, Sweden (NOR, 17.5°E, 60.1°N, 46 masl); and Utö, Finland (UTO, 21.4°E,
153 59.8°N, 8 masl). Sites are equipped with Picarro, Inc. G2401 cavity ring-down spectroscopy gas analysers,
154 providing continuous CH₄ mixing ratios with a mean difference of 0.2 ± 0.8 ppb compared to concurrent flask
155 observations (Levin et al., 2020). The sites discussed here have inlets at heights between 10m and 150m above
156 the ground (Hatakka et al., 2023; ICOS RI et al., 2023).

157

158 Significant enhancements of CH₄ (up to 490 ppb, or ~25%) were detected at each of these sites in the days
159 following the Nord Stream leaks (Figure 3). We compare to the highest altitude inlet for each site, which ranges
160 between 57m and 150m above the ground across the four sites. UTO has only one inlet height, and variations
161 across inlet height at BIR and NOR are less than 0.5 ppb. At HTM's highest inlet (150 masl), observed CH₄
162 mixing ratios quite different (up to 40 ppb) to the two lower inlets and we choose this inlet height to attempt to



163 reduce the impact of boundary layer mixing. There were relatively small CH₄ enhancements at UTO late on the
164 26th September, before larger enhancements were detected at NOR, HTM and finally BIR on the evening of the
165 next day. This distribution is consistent with the CH₄ plume from the leak being transported eastwards and then
166 moving back westwards across Scandinavia before it was detected by IASI off the west coast of Norway on the
167 27th and 28th September. Here we used the data obtained at the ICOS locations for independent verification of
168 our IASI-based analysis of the Nord Stream leaks.

169

170 3. Emission rate estimation methods and model description

171

172 We used two methods to estimate the total mass of CH₄ in the plume observed by IASI. We first applied an
173 integrated mass enhancement (IME) technique, in tandem with Lagrangian model simulations, in order to
174 estimate the total extra mass of CH₄ contained within the plume relative to local background concentrations.
175 The Lagrangian model is used to inform the definition of the ‘plume’ and ‘background’ regions. This method
176 has the advantage that, unlike formal inversions, it is not directly dependent on the accuracy of model transport
177 to quantify the mass of CH₄ in the plume, but the main disadvantage is that it is not possible to exploit the
178 averaging kernels (AKs) of the IASI retrievals to account for the vertical sensitivity of the derived XCH₄, which
179 peaks in the mid-upper troposphere. It also does not account for cloudy regions in which CH₄ is not retrieved.
180 We therefore also employed a formal inverse modelling method based on simulation from a Eulerian chemical
181 transport model which allowed us to model the plume directly and to take account of the satellite AKs.

182

183 The IME methodology used the Hybrid Single Particle Lagrangian Integrated Trajectory (HYSPPLIT) model
184 (Draxler and Hess, 1998) to produce a trajectory analysis which we combined with the XCH₄ data to determine
185 boundaries for the enhanced CH₄ region due to the leaks. The HYSPLIT model was initiated with GFS
186 meteorological data, with forward model trajectories starting at 1 km, 2km and 3km from 00:00 UTC on 26th
187 September, running through to 00:00 UTC on 30th September. All three trajectories showed a similar pathway
188 over the Baltic Sea, crossing Sweden during the morning of the 27th and reaching the Norwegian Sea by the 28th
189 September. These trajectories, along with the IASI observations themselves, were used to define suitable
190 enhanced XCH₄ regions and background regions, which represented the likely XCH₄ without the presence of the
191 Nord Stream plume. The background regions were defined to the west of the calculated plume trajectories, at
192 similar latitude ranges, away from the area affected by the leaks and over the ocean to preclude potential local
193 sources of CH₄. Background and enhancement regions are shown in Figure 2. The total additional CH₄ burden
194 was calculated by computing the difference in the mean XCH₄ concentrations over the two regions and
195 multiplying by the area. Estimates of the uncertainty were derived by perturbing the boundaries of the
196 ‘background’ area chosen in each case with 4 scenarios, adjusting latitude- and longitude-box edges by ± 1
197 degree. We calculated estimates for the scenes observed on the morning of 26th September, the evening of the
198 27th and both the morning and evening of the 28th. The enhanced and background regions were allowed to vary
199 over time as the plume moved and dispersed across the North Sea. Multiple enhancement regions were
200 permitted within a single overpass.

201



202 We also applied an atmospheric inversion technique to the IASI data to produce an optimised time-varying
203 estimate of the emission rate for CH₄ from the leak. We used the global chemical transport model, TOMCAT
204 (Chipperfield, 2006; Monks et al., 2017), to simulate the emission and transport of CH₄ from the location of the
205 leak. TOMCAT has been used in a number of previous studies related to atmospheric CH₄ (e.g. McNorton et al.,
206 2016, 2018; Wilson et al., 2016, 2021; Dowd et al., 2023), along with other atmospheric species. We ran the
207 model at a horizontal resolution of 1.125° × 1.125°, which equates to approximately 65 km (east-west edges) ×
208 125 km (north-south edges) at 60°N. There were 60 vertical levels from the surface up to 0.1 hPa. The model
209 dynamical time step was 5 minutes. The model was forced by meteorological data from the European Centre for
210 Medium-range Weather Forecasts (ECMWF) Operational analyses, regridded to the same horizontal and
211 vertical resolution as the model grid. The meteorological data were read into the model every 6 hours, and
212 linearly interpolated in time for each model time step. The initial conditions were produced from a previous
213 forward simulation which ran up to 00:00 26th September 2022. Our simulation for the inversion ran from this
214 time until 00:00 29th September 2022.

215

216 We simulated all non-plume-related CH₄ transport and chemistry as a separate tracer in the model, with all CH₄
217 fluxes from sources other than Nord Stream included in this background CH₄ tracer. Wetland emissions were
218 taken from the WetCHARTs inventory (Bloom et al., 2017). Anthropogenic emissions were taken from the
219 EDGAR v5 inventory (Crippa et al., 2020), whilst fire emissions were from GFED v4.1s (van der Werf et al.,
220 2017). Emissions from all other sectors, the soil sink of CH₄ and the monthly mean offline atmospheric loss
221 rates were as described in Wilson et al. (2021). Stratospheric loss rates due to O(¹D) and chlorine are taken from
222 a previous TOMCAT full chemistry simulation (Monks et al., 2017) and hydroxyl radical distributions are based
223 on Spivakovsky et al. (2000). The enhanced XCH₄ observed by IASI is large, and the model run is short, so the
224 effect of uncertainties from other sources and sinks of CH₄ should be minimal.

225

226 The emissions from the Nord Stream leak were treated as coming from point sources in the model (at 54.88°N,
227 15.41°E; 55.54°N, 15.60°E; and 55.56°N, 15.79°E), although these were instantly spread across the surface
228 model grid cells containing the leaks. The southernmost leak was located near a model grid cell boundary in the
229 longitudinal direction (at 15.2°E), so this leak was split equally between the two adjacent grid cells. This
230 artificial instantaneous spreading out of the CH₄ from the leak will likely have some effect on the model's
231 representation of the plume movement but is unavoidable in a Eulerian model such as TOMCAT. Leak
232 emissions during each 3-hour time window over the simulation were tagged as separate tracers to allow for
233 independent scaling by the inversion (Figure S1). Figure 4 shows the TOMCAT column-averaged CH₄ at 08:30
234 UTC, the approximate IASI overpass time over the plume.

235

236 We assumed two different *a priori* (prior) emission rate distributions. The first was a constant release rate of
237 4.17 Gg hr⁻¹ (4,170 tonnes hr⁻¹) over the three days, emitting 300 Gg (300,000 tonnes) in total over this time.
238 The second distribution was an exponential decay with an e-folding lifetime of 24 hours, scaled to emit the same
239 total CH₄ over the three days. These prior emission rates are shown in Figure 5. We refer to these as the
240 'constant prior' and the 'decaying prior' throughout this text.

241



242 We carried out Bayesian inversions based on analytical calculation of an *a posteriori* (posterior) leak emission
243 rate based on finding the minimum of a cost function as in Tarantola and Valette (1982). We optimised the
244 mean flux from the leak locations for each 3-hour window throughout the simulation and the mean background
245 XCH₄, giving 25 optimised values in total. The mean background XCH₄ was given a prior uncertainty of 1%,
246 equal to approximately 18 ppb, and was changed very little by the inversion. All other sources and sinks were
247 kept unchanged. We assimilated only the data from the morning of September 28th (Figure 2e), since this
248 overpass detected the most coherent and extensive observation of the plume. We either assimilated all
249 observations made that morning (3980 individual retrievals, denoted ‘all’), or retrievals only within the region
250 bounded by the longitudes 3.5°W and 9.8°E and the latitudes 58.7°N and 70.0°N, the region that contained the
251 main mass of the plume on the morning of 28th September (905 individual retrievals, denoted ‘plume’, see
252 Figure 6a for region definition). The AK associated with each IASI sounding was applied to the corresponding
253 TOMCAT methane profile. Due to the small number of variables that we optimise, and the relatively small
254 number of observations included, the posterior solution can be solved for directly, as has been done previously
255 using TOMCAT (e.g. McNorton et al., 2018; Claxton et al., 2020). See Supplementary Material and those
256 references for more detail of the inversion method.

257

258 We tested both the assumption that the Gaussian emissions uncertainties during each 3-hour window were
259 uncorrelated with each other (nocorr), and that consecutive emission windows had uncertainties with
260 correlations of 0.7 (corr). This value was chosen in order to impose a fairly strong correlation between emission
261 windows but proved to have little impact on results during emission windows that were well-constrained by
262 observations (See Figure 5). We tested prior uncertainties of both 100% and 50% (denoted 1.0σ and 0.5σ).
263 Finally, instead of optimising against the full set of individual IASI retrievals, we tried optimising only the mean
264 XCH₄ value within the bounded region described above (denoted ‘regional mean’). This was intended to
265 account for discrepancies between the simulated location of the plume compared to the observed location. In
266 total we therefore carried out 24 different inversions based on different prior emission distributions, sets of
267 assimilated data, and assumptions regarding prior uncertainties. In all inversions, the uncertainty on the
268 retrievals was set at 30 ppb and were assumed to be uncorrelated with each other. This value is more
269 conservative than the estimated individual IASI sounding uncertainty (~20 ppb), in order to attempt to account
270 for uncertainties from the model transport. We applied the IASI averaging kernels to represent the satellite’s
271 vertical sensitivity in the simulated column average values. The matrices were inverted using LU decomposition
272 methods.

273

274 For comparison of our results with the ICOS CH₄ observations, we interpolate the simulated prior or posterior
275 mixing ratios from all tracers to the corresponding latitude, longitude and inlet heights of the ICOS sites, before
276 adding them together to produce simulated time series of CH₄ at each of the four sites. At each site, we
277 compared to the observational data obtained at the highest inlet height available, to attempt to reduce the
278 influence of boundary layer mixing.

279

280

281



282 **4. Results**

283

284 **4.1 Integrated Mass Enhancement (IME) results**

285

286 The IME method yielded various total mass estimates for each of the overpass times during the first three days
287 of the leak. The results are shown in Table 1. The first estimate of 50 ± 2 Gg CH₄ is from an overpass that
288 occurred only a few hours after the first leak began. Assuming that the leak commenced at 02:00 local time and
289 that IASI was able to view most of the leaked CH₄ during this overpass, this implies a mean emission rate of
290 ~ 6.7 Gg hr⁻¹ during that time. However, many nearby areas were obscured by cloud, so it is likely that IASI
291 could not view all of the CH₄ emitted during these initial hours. The estimate at this time is therefore likely to be
292 an underestimate of the total CH₄ release.

293

294 No plume was visible for the next 36 hours, before what was quite likely only a partial view of the plume
295 obtained on the evening of 27th September on the west coast of Norway. The total CH₄ mass within this plume
296 was 37 ± 1 Gg. A very clear view of the plume, which by this point was beginning to split into northern and
297 southern sections, on the morning of 28th September yielded an inferred total of 394 ± 9 Gg of CH₄. Finally, a
298 total enhancement of 193 ± 6 Gg was calculated for the evening of the 28th.

299

300 Analysis of these values is complex for two reasons. First, the effect of the IASI instrument's vertical sensitivity
301 through application of AKs has not been taken into account. The consequences of this are hard to quantify as
302 they depend on the vertical sensitivities of IASI both within the plume and in the background regions, and the
303 actual vertical distribution of the CH₄ within the column in those regions. Using the TOMCAT model to
304 compare the total column values in the plume with and without the AKs applied indicates that the error due to
305 this effect may be up to 4%, although this relies on the accuracy of the model's vertical transport. Second, it is
306 possible, and on some overpasses likely, that not all of the CH₄ emitted from the leak was viewed by the
307 satellite, which would introduce a negative bias to the results.

308

309



310 Table 1: Integrated mass enhancement (Gg CH₄) calculated from the Nord Stream plume observed by IASI over
 311 three days in September 2022. Also included are the defined enhancement region and background region boundaries.
 312 Overpass times with 'N/A' stated are for overpasses when the satellite's view of the CH₄ plume was obscured by
 313 cloud.

Approximate local overpass time (hh:mm DD/MM/YY)	Enhancement region boundaries	Background region boundaries	Total derived CH ₄ mass enhancement (Gg)
09:30 26/09/22	53°N – 56°N; 13°E – 17°E	64°N – 70°N; -4°E – 0°E	50 ± 2
21:30 26/09/22	N/A	N/A	N/A
09:30 27/09/22	N/A	N/A	N/A
21:30 27/09/22	64°N – 66°N; 8°E – 10°E	64°N – 70°N; -4°E – 0°E	37 ± 1
09:30 28/09/22	1) 59°N – 63°N; -2°E – 4.5°E 2) 63°N – 70°N; 4°E – 7°E 3) 66°N – 71°N; -12°E – -8°E	64°N – 70°N; -12°E – -8°E	394 ± 9
21:30 28/09/22	1) 68°N – 72°N; -8°E – 4.5°E 2) 59°N – 63°N; 1°E – 4°E	64°N – 68°N; -12°E – -8°E	193 ± 6

314
 315
 316



317 **4.2 Inversion results**

318

319 Figure 4 shows the development of the simulated Nord Stream plume in the TOMCAT model over the first
320 three days of the leak, assuming constant emission rates during this time. The plume initially moves northwards
321 and eastwards during the first day. Over the following two days the plume is transported rapidly westwards
322 across Sweden and Norway, before emerging over the North Sea at a similar time and location as indicated by
323 the satellite observations. The plume becomes quite diffuse by the evening of 28th September.

324

325 The prior emissions, in both the ‘constant’ and ‘decaying’ configurations, underestimate the observed XCH₄ in
326 the plume region on the morning of 28th September (Figure 6 and Figures S2 – S4). In addition, the simulated
327 location of the northern section of the plume is slightly east of the observed location. This is likely due to a
328 combination of underestimation of the initial leak rate, errors in the timing of the peak emissions in the prior and
329 model transport errors. It is possible that the meteorological analyses used in the model and the vertical mixing
330 parameterisation in TOMCAT combine to produce small errors in the simulated plume position. Figure 7 shows
331 the total posterior emissions over the first two days of the leaks. In all cases, the posterior emissions are larger
332 than the prior emissions. We report totals for only the first two days, as the observations provided by IASI on
333 the morning of 28th September do not constrain emissions on the third day. The mean posterior emission total
334 for these two days is 282 ± 47 Gg (here the reported uncertainty represents the standard deviation across the
335 mean posterior values). The mean posterior total is 255 ± 30 Gg when omitting the ‘regional mean’ inversions
336 where only the mean CH₄ value is optimised. However, there is significant variation in the posterior totals,
337 which range between 215 ± 13 Gg and 374 ± 50 Gg, depending on the assumptions made (here the uncertainty
338 represents the derived posterior uncertainty from the individual inversion). Total posterior emissions are
339 consistently smaller when applying the ‘decaying’ prior than with the ‘constant’ prior, whilst posterior
340 emissions are largest when optimising against only the regional mean, rather than against individual retrievals.

341

342 When the inversion optimises the model using the individual IASI retrievals, the position of the northern section
343 of the plume is improved (moved further west), similar to the observations (Figure 6 and Figures S2 – S4), and
344 simulated XCH₄ is increased. However, the XCH₄ still remains lower than the observed values. When the
345 regional mean is optimised, the magnitudes of the simulated XCH₄ values are much improved, but the position
346 of the largest values is not improved relative to the IASI observations. The remaining errors in the model
347 representation of the plume are likely due to: i) errors in the ECMWF meteorological data, which might be
348 improved through use of reanalyses rather than the operational analyses; ii) biases in the model transport
349 parameterisations, particularly for vertical mixing, leading to incorrect simulated vertical distribution of the
350 plume; and iii) uncertainties produced due to the instantaneous mixing of the leak emissions across model grid
351 boxes.

352

353 The three-hourly posterior emission rates display significant variation over the first two days of the leaks
354 (Figure 5). Whether the ‘constant’ or ‘decaying’ prior are used, there are three peaks in the posterior flux rates –
355 the first during the early afternoon on the 26th September, and two more smaller peaks during the morning and
356 afternoon of the 27th. There are low emission rates between these times. This temporal variation is consistent



357 across all inversions, including, to some extent, when only the regional mean XCH₄ is optimised (Figure S5).
358 The posterior emissions are far outside of the prior uncertainty during peak flux rates and, in fact, are below
359 zero during the night of 26th. This negative flux is also suggestive of model transport errors. Unless temporal
360 error correlations are included for the prior flux in an inversion, emissions during the third day are not
361 constrained.

362

363 Figure 3 includes the CH₄ mixing ratios observed at the four ICOS sites for 26th – 29th September, and the prior
364 and posterior model values at those locations. The largest observed CH₄ enhancements above the background
365 concentrations were at BIR (~500 ppb), with enhancements of ~340 ppb at NOR and HTM and much smaller
366 enhancements of less than 60 ppb at UTO. The prior model simulations are close to the observations at UTO. At
367 BIR, the peaks in the prior simulations have magnitudes close to the observed value but occur around 3 hours
368 too early. The timing of the peak in the prior simulation at NOR is similarly early and the magnitude is 200 –
369 700 ppb too high. Finally, the model performance at HTM is poor, with very large simulated values, likely due
370 to the site's location relative to the model grid boundaries and the fast spreading of the leak emissions both
371 leading to excessive influence from CH₄ directly from the leaks. In general, the IASI-based posterior emissions
372 do not improve the model performance at the ICOS sites. Peak CH₄ at each site, which tended to be too large in
373 the prior simulations, has generally remained the same or increased. Posterior values at HTM have significantly
374 increased, whilst performance at UTO has changed little. At NOR and BIR, the posterior peaks remain too
375 large, although the timing of the plume reaching BIR has improved in the inversions that optimised against the
376 individual retrievals. At all sites, the large emissions inferred from the inversions that optimised the mean XCH₄
377 in the plume produce very large simulated mixing ratios at the ICOS sites.

378

379 5. Discussion

380

381 The range of estimates from both of the methodologies that we applied to estimate the total CH₄ emitted from
382 the Nord Stream leaks using IASI retrievals of XCH₄ produced values greater than 200 Gg, with some estimates
383 reaching almost twice that value. A leak of this magnitude is by far the largest individual anthropogenic leak of
384 CH₄ to the atmosphere on record, at least twice as large as the previous largest emission event in Aliso Canyon,
385 California in 2015-2016 (97 Gg, Conley et al. (2016)). That leak was from a ruptured injection well pipe at a gas
386 storage facility near Los Angeles and continued for more than three months.

387

388 The magnitude of the Nord Stream leaks is highly significant on a global scale – when considered over a short
389 period. Total global CH₄ emissions from fossil fuels amounted to 108 Tg in the year 2017 (Saunio et al. (2020),
390 top-down estimate), or approximately 300 Gg day⁻¹. Our mean estimate from the Nord Stream leaks over two
391 days is therefore approximately equivalent to an extra day's emissions from global fossil fuel sources (although
392 it should be noted that daily emissions are likely larger today than they were in 2017). However, in the context
393 of annual anthropogenic CH₄ emissions (~364 Tg yr⁻¹), the Nord Stream leaks contributed only an extra 0.08%,
394 and increased the annual global total CH₄ emissions from all sources (~600 Tg yr⁻¹) by just 0.05%. Chen and
395 Zhou (2023) calculated that a leak from Nord Stream of magnitude 220 Gg would have a negligible warming



396 effect on the climate ($1.8 \times 10^{-5} \text{°C}$ over a 20-year time period) and our slightly larger emission estimates would
397 have a correspondingly small effect.

398

399 IASI had its best view of the plume during the morning of 28th September 2022, and we base our best estimate
400 of the total CH₄ leaked to the atmosphere during the preceding two days on the observations made at that time.

401 Our IME method produced a value of 390 Gg CH₄ from those retrievals, whilst our TOMCAT inversion results
402 produced a range of 215 - 374 Gg, with a mean of 255 ± 30 Gg when optimising the model based on

403 comparisons to individual retrievals. The consistency between the results produced using the two methods is

404 therefore heavily dependent on the assumptions made during the inversion process, but the IME value is

405 approximately 50% larger than the inversion mean. This is likely due in part to the fact that the posterior

406 simulations still produce smaller XCH₄ values in the region of the plume than those observed by IASI,

407 indicating that the inversion-derived posterior total flux might still be too small. Indeed, the inversions that

408 optimise the simulated regional mean XCH₄ values rather than individual retrievals of XCH₄ produce posterior

409 emission totals (301 – 374 Gg) much closer to that derived by the IME method, and posterior XCH₄ values

410 similar to those observed by the satellite, albeit located too far east. In addition, the IME method does not take

411 account of IASI's vertical sensitivity and it is not known how results are affected by this. The effect of missing

412 IASI data due to cloud cover on the estimated IME value (and to a lesser extent, on the inversions) is also

413 difficult to quantify.

414

415 We investigated the vertical structure of the simulated plume, together with the vertical sensitivity of XCH₄

416 retrievals based on the IASI AKs (Figure S6). This shows that the northern and southern sections of the plume

417 during the morning of 28th September (defined as 66°N – 71°N, -5°E – 6°E and 59°N – 63°N, 0°E – 7°E,

418 respectively) have different vertical structures in the model. The northern section has high near-surface CH₄

419 mixing ratios from the leaks, which remain relatively constant as with altitude before decreasing until there is no

420 influence from Nord Stream above 500 hPa (~5.5 km). In this case, the majority of the leak-related CH₄ is

421 located beneath the peak IASI vertical sensitivity indicated by the AKs. Meanwhile, in the southern section, the

422 CH₄ contribution from the leak is smaller, but peaks higher up, at approximately 600 hPa (~4 km), around the

423 same region as the peak satellite sensitivity. If the vertical distributions produced in the model are correct, this

424 indicates that the observed XCH₄ in the northern and southern sections of the plume, whilst displaying similar

425 XCH₄ values, are in fact due to very different relative CH₄ contributions within the column. If the simulated

426 vertical distributions are correct, it is likely that the IME method underestimates the CH₄ mass in the northern

427 section of the plume whilst overestimating it in the southern section.

428

429 The interpretation that the inversion-derived values are low is complicated by the fact that both the prior and the

430 posterior simulations produce larger-than-observed CH₄ mixing ratios at the ICOS site locations (Figure 3). In

431 the model, the HTM site is located in a grid box next to the one into which the Nord Stream CH₄ is emitted, and

432 the comparison there is likely negatively and unrealistically affected by this. However, the simulated mixing

433 ratios at NOR and BIR are generally too large when using the prior emissions, and substantially larger when

434 using the posterior emissions. In fact, an inversion based only on assimilating the ICOS observations, without

435 the IASI data, produces a much smaller posterior total emission (88 ± 13 Gg, Figure S7). We hypothesise that



436 our Eulerian model's representation uncertainty is large when simulating the movement of a large distinct plume
437 over fixed point measurement locations, especially at the resolution used here. In addition, the model's
438 representation of the detailed vertical structure of the plume is key for such comparisons. The use of a high-
439 resolution regional model, a nested grid, or a Lagrangian model might produce better comparisons at the ICOS
440 sites.

441

442 Our IASI-based estimates are consistently larger than estimates produced by others using different observational
443 datasets. Previous estimates issued by our team and by other groups were produced quickly in the weeks
444 immediately following the leaks, and we have here attempted to probe the sensitivity of our results to chosen
445 methodologies and assumptions about the leaks and observational data. Based on ICOS observations, satellite-
446 based imaging spectrometer data and multiple Lagrangian models, Jia et al. (2022) calculated a total flux of 220
447 ± 30 Gg CH_4 over three days of leaks, which itself was larger than many estimates published by various groups
448 using a range of methods and datasets (CAMS, 2022; NILU, 2022; UNEP & IMEO, 2023). The temporal
449 variation of emissions produced by Jia et al. (2022) showed some similarity to our own results, with the peak
450 emission rate occurring during the night of 26th -27th September, more than 24 hours after the leaks began. They
451 also computed the mass of CH_4 that was released from the pipelines based on pipeline dimensions and the
452 change in gas pressure within the pipes, calculating a value of 230 Gg. This value, along with their calculated
453 emission value, is smaller than the majority of our emission estimates, although a subset of our results is
454 consistent with their value. It remains important to investigate the roots of the apparent discrepancies between
455 our IASI-derived estimates and those produced via other means.

456

457 The resolution used by TOMCAT in this case (approximately $1^\circ \times 1^\circ$), is fairly coarse for capturing the
458 movement of the plume over the ICOS sites in particular, and results will be affected by the artificial
459 instantaneous spreading of the point source emissions over the comparatively large model grid cells. We can
460 employ Eulerian models with higher resolution, and/or Lagrangian plume models, to attempt to better represent
461 the plume's distribution in comparison with IASI. The effect of the meteorological data used in the models can
462 also be assessed through the use of reanalyses from ECMWF or other meteorological datasets. The operational
463 meteorological analyses used here are updated by ECMWF during reanalysis through assimilation of satellite
464 and *in situ* observations, which might result in better consistency between the simulated and observed plume. In
465 addition, investigation into the model's representation of plume uplift above the CH_4 release to the atmosphere
466 might be a key uncertainty, since it determines layer height and therefore the horizontal wind field to which the
467 simulated plume is exposed.

468

469 6. Summary and Conclusions

470

471 We have produced the first clear satellite retrievals of column average methane that capture the CH_4 emitted
472 into the atmosphere from the Nord Stream gas leaks in late September 2022. The IASI instrument, onboard the
473 satellite MetOp-B, produced retrievals displaying strongly enhanced XCH_4 at the leak locations on the morning
474 of 26th September, before large widespread enhancements were seen over the North Sea during 28th September.



475 The satellite data retrieved for that day allowed us to employ two methods to quantify the CH₄ leaked to the
476 atmosphere from the Nord Stream leaks during the first two days.

477

478 Our integrated mass enhancement calculations produced total emissions of 200 – 390 Gg CH₄, although this
479 method cannot take account of the satellite instrument's vertical sensitivity, which peaks in the mid-upper
480 troposphere, and cannot account for regions of enhanced CH₄ that are not observed due to clouds. We also used
481 formal Bayesian inversion methods, using the TOMCAT atmospheric chemical transport model, to quantify the
482 emissions based on the observations made on the morning of 28th September. This is the first time that plume
483 flux inversions have been carried out using thermal infrared satellite data. Here, we investigated the effect of a
484 range of assumptions within the inversion, including the prior distribution of the emissions, the related prior
485 uncertainties and the way that observations are assimilated. We calculated total emissions between 215 and 374
486 Gg. The mean over all inversions is approximately 282 ± 47 Gg, whilst the mean over the inversions that
487 optimise against individual IASI retrievals is 255 ± 30 Gg. All of our results imply that the Nord Stream leaks
488 were by far the largest recorded individual anthropogenic leak of CH₄ to the atmosphere.

489

490 Our estimates are larger than previous values given for the Nord Stream leaks, produced using alternative
491 observational data. There are large differences between our posterior results and *in situ* observations made in the
492 region, and more work is necessary to discern to what extent this is due to errors in the flux estimates produced
493 from the satellite data and how much is due to poor model plume representation at the tall tower locations. Our
494 ability to monitor, simulate and quantify leaks of GHGs and pollution events such as this one is continuously
495 improving, aiding our ability to mitigate the human influence on the atmosphere. It is also clear from this study
496 that thermal infrared instruments such as IASI, which have peak sensitivity high in the troposphere, are able to
497 provide more information concerning surface events such as the Nord Stream leaks than might have been
498 appreciated previously. In any case, whilst this particular event remains highly significant locally over a short
499 time period, the effect of these emissions, by themselves, is very small in terms of both the global atmospheric
500 CH₄ budget and the climate.

501

502 **Data Availability**

503

504 MetOp-B IASI methane observations up to March 2021 are available on the Centre for Environmental Data
505 Analysis (CEDA) long-term data archive (Knappett et al., 2022). More recent data, including the near-real time
506 (NRT) data for the period covering the Nord Stream leaks, is viewable through the public visualisation tool
507 (<http://rsg.rl.ac.uk/vistool>, last access 18/07/2023). NRT data is available through contacting the authors. The
508 TOMCAT model output for this period will be made available on the Centre for Environmental Data Analysis
509 (CEDA) long-term data archive upon publication of this work. The ICOS methane concentrations were
510 downloaded from ICOS Carbon portal (<https://data.icos-cp.eu/portal/>, last access 18/07/2023).

511

512

513

514



515 **Author contribution**

516

517 CW, BJK, and JJR conceptualised the study. BJK, RS, and LJV produced the satellite data. CJW, DPM, ED,

518 WF and MPC carried out data analysis and modelling. All co-authors contributed to the design of the study and

519 to writing the manuscript.

520

521

522 **Competing interests**

523

524 The authors declare that they have no conflict of interest.

525

526 **Acknowledgements**

527

528 This work was funded by the Natural Environment Research Council through its grants to the UK National

529 Centre for Earth Observation (NCEO; NERC grant numbers NE/R016518/1 and NE/N018079/1). The IASI

530 retrievals were produced using JASMIN, the UK collaborative data analysis facility, at the Rutherford Appleton

531 Laboratory. The TOMCAT model simulations were carried out using ARC4, part of the High-Performance

532 Computing facilities at the University of Leeds, UK. EUMETSAT provided data for MetOp-B IASI, MHS &

533 AMSU-A data and ECMWF provided meteorological data used in NRT processing system and TOMCAT

534 simulations. We thank ICOS PIs for providing their methane concentration data.

535

536



537 **References**

- 538
539 Bloom, A. A., Bowman, K. W., Lee, M., Turner, A. J., Schroeder, R., Worden, J. R., Weidner, R., McDonald,
540 K. C., and Jacob, D. J.: A global wetland methane emissions and uncertainty dataset for atmospheric chemical
541 transport models (WetCHARTs version 1.0), *Geoscientific Model Development*, 10, 2141–2156,
542 <https://doi.org/10.5194/gmd-10-2141-2017>, 2017.
- 543 Blumstein, D., Chalon, G., Carlier, T., Buil, C., Hebert, P., Maciaszek, T., Ponce, G., Phulpin, T., Tournier, B.,
544 Simeoni, D., Astruc, P., Clauss, A., Kayal, G., and Jegou, R.: IASI instrument: technical overview and
545 measured performances, *Infrared Spaceborne Remote Sensing XII*, 5543, 196–207,
546 <https://doi.org/10.1117/12.560907>, 2004.
- 547 Buchwitz, M., Schneising, O., Vanselow, S., Houweling, S., van Peet, J., Siddans, R., Kerridge, B., Ventress,
548 L., Knappett, D., Crevoisier, C., Meilhac, N., Borsdorf, T., Lorente, A., and Aben, I.: Methane+ Study Final
549 Report, ESA Contract No. 4000129987/20/I-DT, <https://methanepius.eu>, 2023.
- 550 CAMS: Copernicus Atmosphere Monitoring Service (CAMS) simulates methane emissions from Nord Stream
551 pipelines leaks, [https://atmosphere.copernicus.eu/cams-simulates-methane-emissions-nord-stream-pipelines-](https://atmosphere.copernicus.eu/cams-simulates-methane-emissions-nord-stream-pipelines-leaks)
552 [leaks](https://atmosphere.copernicus.eu/cams-simulates-methane-emissions-nord-stream-pipelines-leaks), 2022.
- 553 Chen, X. and Zhou, T.: Negligible Warming Caused by Nord Stream Methane Leaks, *Adv. Atmos. Sci.*, 40,
554 549–552, <https://doi.org/10.1007/s00376-022-2305-x>, 2023.
- 555 Chipperfield, M. P.: New version of the TOMCAT/SLIMCAT off-line chemical transport model:
556 Intercomparison of stratospheric tracer experiments, *Quarterly Journal of the Royal Meteorological Society*,
557 132, 1179–1203, <https://doi.org/10.1256/qj.05.51>, 2006.
- 558 Claxton, T., Hossaini, R., Wilson, C., Montzka, S. A., Chipperfield, M. P., Wild, O., Bednarz, E. M., Carpenter,
559 L. J., Andrews, S. J., Hackenberg, S. C., Mühle, J., Oram, D., Park, S., Park, M.-K., Atlas, E., Navarro, M.,
560 Schaufli, S., Sherry, D., Vollmer, M., Schuck, T., Engel, A., Krummel, P. B., Maione, M., Arduini, J., Saito,
561 T., Yokouchi, Y., O’Doherty, S., Young, D., and Lunder, C.: A Synthesis Inversion to Constrain Global
562 Emissions of Two Very Short Lived Chlorocarbons: Dichloromethane, and Perchloroethylene, *Journal of*
563 *Geophysical Research: Atmospheres*, 125, e2019JD031818, <https://doi.org/10.1029/2019JD031818>, 2020.
- 564 Conley, S., Franco, G., Faloona, I., Blake, D. R., Peischl, J., and Ryerson, T. B.: Methane emissions from the
565 2015 Aliso Canyon blowout in Los Angeles, CA, *Science*, 351, 1317–1320,
566 <https://doi.org/10.1126/science.aaf2348>, 2016.
- 567 Crippa, M., Solazzo, E., Huang, G., Guizzardi, D., Koffi, E., Muntean, M., Schieberle, C., Friedrich, R., and
568 Janssens-Maenhout, G.: High resolution temporal profiles in the Emissions Database for Global Atmospheric
569 Research, *Scientific Data*, 7, 121, <https://doi.org/10.1038/s41597-020-0462-2>, 2020.
- 570 Danish Energy Agency: Leak at North Stream 2 in the Baltic Sea, [https://ens.dk/en/press/leak-north-stream-2-](https://ens.dk/en/press/leak-north-stream-2-baltic-sea)
571 [baltic-sea](https://ens.dk/en/press/leak-north-stream-2-baltic-sea), 2022.



- 572 Dowd, E., Wilson, C., Chipperfield, M. P., Gloor, E., Manning, A., and Doherty, R.: Decreasing seasonal cycle
573 amplitude of methane in the northern high latitudes being driven by lower-latitude changes in emissions and
574 transport, *Atmospheric Chemistry and Physics*, 23, 7363–7382, <https://doi.org/10.5194/acp-23-7363-2023>,
575 2023.
- 576 Draxler, R. R. and Hess, G. D.: An overview of the HYSPLIT_4 modelling system for trajectories, dispersion
577 and deposition., *Aust. Met. Mag.*, 47, 295–308, 1998.
- 578 European Commission: Joint EU-US Press Release on the Global Methane Pledge,
579 https://ec.europa.eu/commission/presscorner/detail/en/IP_21_4785, 2021.
- 580 GEUS: GEUS har registreret rystelser i Østersøen (GEUS has registered tremors in the Baltic Sea),
581 <https://www.geus.dk/om-geus/nyheder/nyhedsarkiv/2022/sep/seismologi>, De Nationale Geologiske
582 Undersøgelser for Danmark og Grønland, 2022.
- 583 GHGSat: GHGSat measures its largest emission from a single source ever from Nord Stream 2 leak,
584 <https://www.ghgsat.com/en/newsroom/ghgsat-nordstream/>, 2022.
- 585 Hatakka, J., Laurila, T., and ICOS, R.: ICOS Atmosphere Level 2 data, Utö - Baltic sea, release 2023-1,
586 <https://doi.org/10.18160/9JJC-CDJW>, 2023.
- 587 Heiskanen, J., Brümmner, C., Buchmann, N., Calfapietra, C., Chen, H., Gielen, B., Gkritzalis, T., Hammer, S.,
588 Hartman, S., Herbst, M., Janssens, I. A., Jordan, A., Juurola, E., Karstens, U., Kasurinen, V., Kruijt, B.,
589 Lankreijer, H., Levin, I., Linderson, M.-L., Loustau, D., Merbold, L., Myhre, C. L., Papale, D., Pavelka, M.,
590 Pilegaard, K., Ramonet, M., Rebmann, C., Rinne, J., Rivier, L., Saltikoff, E., Sanders, R., Steinbacher, M.,
591 Steinhoff, T., Watson, A., Vermeulen, A. T., Vesala, T., Vítková, G., and Kutsch, W.: The Integrated Carbon
592 Observation System in Europe, *Bulletin of the American Meteorological Society*, 103, E855–E872,
593 <https://doi.org/10.1175/BAMS-D-19-0364.1>, 2022.
- 594 ICOS RI, Apadula, F., Arnold, S., Bergamaschi, P., Biermann, T., Chen, H., Colomb, A., Conil, S., Couret, C.,
595 Cristofanelli, P., De Mazière, M., Delmotte, M., Emmenegger, L., Forster, G., Frumau, A., Hatakka, J., Heliasz,
596 M., Heltai, D., Hensen, A., Hermansen, O., Hoheisel, A., Kneuer, T., Komínková, K., Kubistin, D., Laurent, O.,
597 Laurila, T., Lehner, I., Lehtinen, K., Leskinen, A., Leuenberger, M., Levula, J., Lindauer, M., Lopez, M., Lund
598 Myhre, C., Lunder, C., Mammarella, I., Manca, G., Manning, A., Marek, M., Marklund, P., Meinhardt, F.,
599 Mölder, M., Müller-Williams, J., O'Doherty, S., Ottosson-Löfvenius, M., Piacentino, S., Pichon, J.-M., Pitt, J.,
600 Platt, S. M., Plaß-Dülmer, C., Ramonet, M., Rivas-Soriano, P., Roulet, Y.-A., Scheeren, B., Schmidt, M.,
601 Schumacher, M., Sha, M. K., Smith, P., Stanley, K., Steinbacher, M., Sørensen, L. L., Trisolino, P., Vítková, G.,
602 Yver-Kwok, C., and di Sarra, A.: ICOS Atmosphere Release 2023-1 of Level 2 Greenhouse Gas Mole Fractions
603 of CO₂, CH₄, N₂O, CO, meteorology and 14CO₂, and flask samples analysed for CO₂, CH₄, N₂O, CO, H₂
604 and SF₆, <https://doi.org/10.18160/VXCS-95EV>, 2023.
- 605 Jia, M., Li, F., Zhang, Y., Wu, M., Li, Y., Feng, S., Wang, H., Chen, H., Ju, W., Lin, J., Cai, J., Zhang, Y., and
606 Jiang, F.: The Nord Stream pipeline gas leaks released approximately 220,000 tonnes of methane into the



- 607 atmosphere, *Environmental Science and Ecotechnology*, 12, 100210, <https://doi.org/10.1016/j.ese.2022.100210>,
608 2022.
- 609 Knappett, D., Siddans, R., Ventress, L., Kerridge, B., and Latter, B.: STFC RAL methane retrievals from IASI
610 on board MetOp-B, version 2.0, <https://doi.org/10.5285/4bbcb1722f2842c1b0a5ebc19160a863>, 2022.
- 611 Lauvaux, T., Giron, C., Mazzolini, M., d'Aspremont, A., Duren, R., Cusworth, D., Shindell, D., and Ciais, P.:
612 Global assessment of oil and gas methane ultra-emitters, *Science*, 375, 557–561,
613 <https://doi.org/10.1126/science.abj4351>, 2022.
- 614 Levin, I., Karstens, U., Eritt, M., Maier, F., Arnold, S., Rzesanke, D., Hammer, S., Ramonet, M., Vítková, G.,
615 Conil, S., Heliasz, M., Kubistin, D., and Lindauer, M.: A dedicated flask sampling strategy developed for
616 Integrated Carbon Observation System (ICOS) stations based on CO₂ and CO measurements and Stochastic
617 Time-Inverted Lagrangian Transport (STILT) footprint modelling, *Atmospheric Chemistry and Physics*, 20,
618 11161–11180, <https://doi.org/10.5194/acp-20-11161-2020>, 2020.
- 619 McNorton, J., Gloor, E., Wilson, C., Hayman, G. D., Gedney, N., Comyn-Platt, E., Marthews, T., Parker, R. J.,
620 Boesch, H., and Chipperfield, M. P.: Role of regional wetland emissions in atmospheric methane variability,
621 *Geophysical Research Letters*, 43, 11,433–11,444, <https://doi.org/10.1002/2016GL070649>, 2016.
- 622 McNorton, J., Wilson, C., Gloor, M., Parker, R. J., Boesch, H., Feng, W., Hossaini, R., and Chipperfield, M. P.:
623 Attribution of recent increases in atmospheric methane through 3-D inverse modelling, *Atmospheric Chemistry
624 and Physics*, 18, 18149–18168, <https://doi.org/10.5194/acp-18-18149-2018>, 2018.
- 625 Monks, S. A., Arnold, S. R., Hollaway, M. J., Pope, R. J., Wilson, C., Feng, W., Emmerson, K. M., Kerridge, B.
626 J., Latter, B. L., Miles, G. M., Siddans, R., and Chipperfield, M. P.: The TOMCAT global chemical transport
627 model v1.6: description of chemical mechanism and model evaluation, *Geoscientific Model Development*, 10,
628 3025–3057, <https://doi.org/10.5194/gmd-10-3025-2017>, 2017.
- 629 NCEO: National Centre for Earth Observation: 220,000 tonnes of methane likely released from Nord Stream
630 gas leak, <https://www.nceo.ac.uk/article/220000-tonnes-of-methane-likely-released-from-nord-stream-gas-leak/>,
631 2022.
- 632 NILU: The Climate and Environmental Research Institute (NILU), Norway: Improved estimates of Nord Stream
633 leaks, <https://www.nilu.com/2022/10/improved-estimates-of-nord-stream-leaks/>, 2022.
- 634 Pimlott, M. A., Pope, R. J., Kerridge, B. J., Latter, B. G., Knappett, D. S., Heard, D. E., Ventress, L. J., Siddans,
635 R., Feng, W., and Chipperfield, M. P.: Investigating the global OH radical distribution using steady-state
636 approximations and satellite data, *Atmospheric Chemistry and Physics*, 22, 10467–10488,
637 <https://doi.org/10.5194/acp-22-10467-2022>, 2022.
- 638 Pope, R. J., Kerridge, B. J., Siddans, R., Latter, B. G., Chipperfield, M. P., Arnold, S. R., Ventress, L. J.,
639 Pimlott, M. A., Graham, A. M., Knappett, D. S., and Rigby, R.: Large Enhancements in Southern Hemisphere



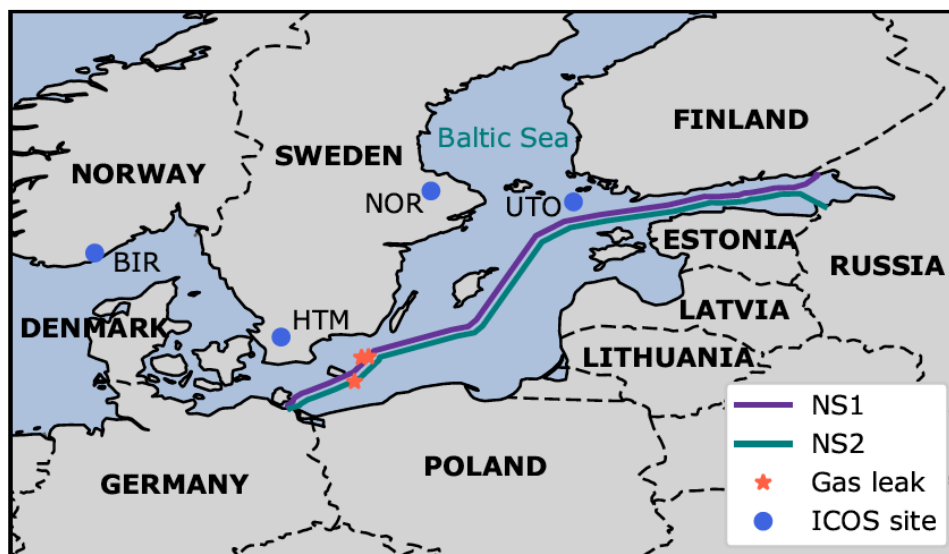
- 640 Satellite-Observed Trace Gases Due to the 2019/2020 Australian Wildfires, *Journal of Geophysical Research:*
641 *Atmospheres*, 126, e2021JD034892, <https://doi.org/10.1029/2021JD034892>, 2021.
- 642 Robson, J., Aksenov, Y., Bracegirdle, T. J., Dimdore-Miles, O., Griffiths, P. T., Grosvenor, D. P., Hodson, D. L.
643 R., Keeble, J., MacIntosh, C., Megann, A., Osprey, S., Povey, A. C., Schröder, D., Yang, M., Archibald, A. T.,
644 Carslaw, K. S., Gray, L., Jones, C., Kerridge, B., Knappett, D., Kuhlbrodt, T., Russo, M., Sellar, A., Siddans,
645 R., Sinha, B., Sutton, R., Walton, J., and Wilcox, L. J.: The Evaluation of the North Atlantic Climate System in
646 UKESM1 Historical Simulations for CMIP6, *Journal of Advances in Modeling Earth Systems*, 12,
647 e2020MS002126, <https://doi.org/10.1029/2020MS002126>, 2020.
- 648 Saunio, M., Stavert, A. R., Poulter, B., Bousquet, P., Canadell, J. G., Jackson, R. B., Raymond, P. A.,
649 Dlugokencky, E. J., Houweling, S., Patra, P. K., Ciais, P., Arora, V. K., Bastviken, D., Bergamaschi, P., Blake,
650 D. R., Brailsford, G., Bruhwiler, L., Carlson, K. M., Carrol, M., Castaldi, S., Chandra, N., Crevoisier, C., Crill,
651 P. M., Covey, K., Curry, C. L., Etiope, G., Frankenberg, C., Gedney, N., Hegglin, M. I., Höglund-Isaksson, L.,
652 Hugelius, G., Ishizawa, M., Ito, A., Janssens-Maenhout, G., Jensen, K. M., Joos, F., Kleinen, T., Krummel, P.
653 B., Langenfelds, R. L., Laruelle, G. G., Liu, L., Machida, T., Maksyutov, S., McDonald, K. C., McNorton, J.,
654 Miller, P. A., Melton, J. R., Morino, I., Müller, J., Murguía-Flores, F., Naik, V., Niwa, Y., Noce, S., O'Doherty,
655 S., Parker, R. J., Peng, C., Peng, S., Peters, G. P., Prigent, C., Prinn, R., Ramonet, M., Regnier, P., Riley, W. J.,
656 Rosentreter, J. A., Segers, A., Simpson, I. J., Shi, H., Smith, S. J., Steele, L. P., Thornton, B. F., Tian, H.,
657 Tohjima, Y., Tubiello, F. N., Tsuruta, A., Viovy, N., Voulgarakis, A., Weber, T. S., van Weele, M., van der
658 Werf, G. R., Weiss, R. F., Worthy, D., Wunch, D., Yin, Y., Yoshida, Y., Zhang, W., Zhang, Z., Zhao, Y.,
659 Zheng, B., Zhu, Q., Zhu, Q., and Zhuang, Q.: The Global Methane Budget 2000–2017, *Earth Syst. Sci. Data*,
660 12, 1561–1623, <https://doi.org/10.5194/essd-12-1561-2020>, 2020.
- 661 Siddans, R., Knappett, D., Kerridge, B., Waterfall, A., Hurley, J., Latter, B., Boesch, H., and Parker, R.: Global
662 height-resolved methane retrievals from the Infrared Atmospheric Sounding Interferometer (IASI) on MetOp,
663 *Atmospheric Measurement Techniques*, 10, 4135–4164, <https://doi.org/10.5194/amt-10-4135-2017>, 2017.
- 664 Spivakovsky, C. M., Logan, J. A., Montzka, S. A., Balkanski, Y. J., Foreman-Fowler, M., Jones, D. B. A.,
665 Horowitz, L. W., Fusco, A. C., Brenninkmeijer, C. a. M., Prather, M. J., Wofsy, S. C., and McElroy, M. B.:
666 Three-dimensional climatological distribution of tropospheric OH: Update and evaluation, *Journal of*
667 *Geophysical Research: Atmospheres*, 105, 8931–8980, <https://doi.org/10.1029/1999JD901006>, 2000.
- 668 Szopa, S., Naik, V., Adhikary, B., Artaxo, P., Berntsen, T., Collins, W. D., Fuzzi, S., Gallardo, L., Kiendler-
669 Schar, A., Klimont, Z., Liao, H., Unger, N., and Zanis, P.: Chapter 6. Short-Lived Climate Forcers, in: *Climate*
670 *Change 2021: The Physical Science Basis. Contribution of Working Group I to the Sixth Assessment Report of*
671 *the Intergovernmental Panel on Climate Change [Masson-Delmotte, V., P. Zhai, A. Pirani, S.L. Connors, C.*
672 *Péan, S. Berger, N. Caud, Y. Chen, L. Goldfarb, M.I. Gomis, M. Huang, K. Leitzell, E. Lonnoy, J.B.R.*
673 *Matthews, T.K. Maycock, T. Waterfield, O. Yelekçi, R. Yu, and B. Zhou (eds.)*], Cambridge University Press,
674 Cambridge, United Kingdom and New York, NY, USA, 817–922, 2021.



- 675 Tarantola, A. and Valette, B.: Generalized nonlinear inverse problems solved using the least squares criterion,
676 *Reviews of Geophysics*, 20, 219–232, <https://doi.org/10.1029/RG020i002p00219>, 1982.
- 677 UNEP & IMEO: United Nations Environment Programme & International Methane Emissions Observatory:
678 Estimate of Total Methane Emissions from the Nord Stream Gas Leak Incident - Draft Working Paper,
679 <https://wedocs.unep.org/20.500.11822/41838>, 2023.
- 680 UNFCCC: United Nations Framework Convention on Climate Change Paris Agreement,
681 <https://unfccc.int/process-and-meetings/the-paris-agreement/the-paris-agreement>, 2015.
- 682 van der Werf, G. R., Randerson, J. T., Giglio, L., Leeuwen, T. T. van, Chen, Y., Rogers, B. M., Mu, M., Marle,
683 M. J. E. van, Morton, D. C., Collatz, G. J., Yokelson, R. J., and Kasibhatla, P. S.: Global fire emissions
684 estimates during 1997–2016, *Earth System Science Data*, 9, 697–720, <https://doi.org/10.5194/essd-9-697-2017>,
685 2017.
- 686 West, J. J., Fiore, A. M., Horowitz, L. W., and Mauzerall, D. L.: Global health benefits of mitigating ozone
687 pollution with methane emission controls, *Proceedings of the National Academy of Sciences*, 103, 3988–3993,
688 <https://doi.org/10.1073/pnas.0600201103>, 2006.
- 689 Wilson, C., Gloor, M., Gatti, L. V., Miller, J. B., Monks, S. A., McNorton, J., Bloom, A. A., Basso, L. S., and
690 Chipperfield, M. P.: Contribution of regional sources to atmospheric methane over the Amazon Basin in 2010
691 and 2011, *Global Biogeochemical Cycles*, 30, 400–420, <https://doi.org/10.1002/2015GB005300>, 2016.
- 692 Wilson, C., Chipperfield, M. P., Gloor, M., Parker, R. J., Boesch, H., McNorton, J., Gatti, L. V., Miller, J. B.,
693 Basso, L. S., and Monks, S. A.: Large and increasing methane emissions from eastern Amazonia derived from
694 satellite data, 2010–2018, *Atmospheric Chemistry and Physics*, 21, 10643–10669, <https://doi.org/10.5194/acp-21-10643-2021>, 2021.
- 696
- 697

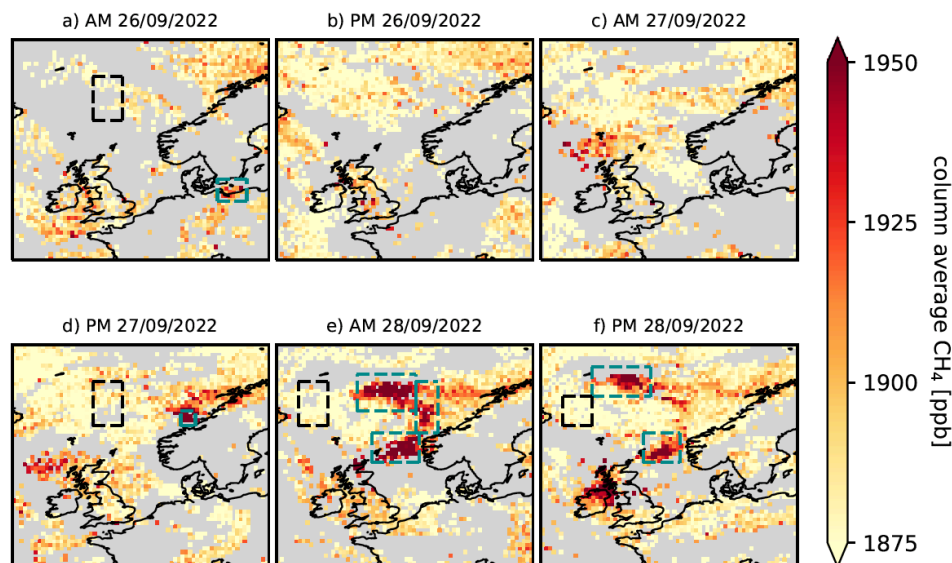


698 **Figures**
699

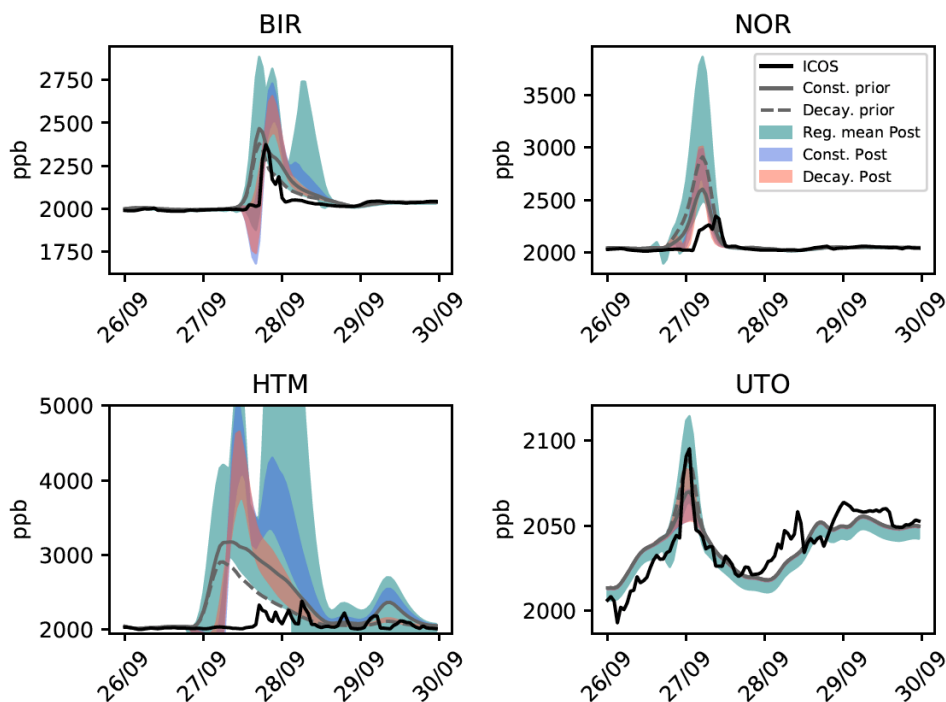


700
701 Figure 1: Map showing Nord Stream pipeline routes (teal and purple lines), gas leak locations (red stars) and *in situ*
702 ICOS monitoring site locations (blue circles).

703



704
705 Figure 2: IASI column average CH₄ (ppb) for 26th - 28th September 2022. Retrievals are averaged onto 0.25° × 0.25°
706 grid boxes, weighted inversely to their uncertainties for the morning and evening overpasses of each day. Black
707 dashed boxes show 'background' regions used in the integrated mass enhancement (IME) method, whilst turquoise
708 dashed boxes show 'enhancement' regions. Grey regions are obscured by cloud.

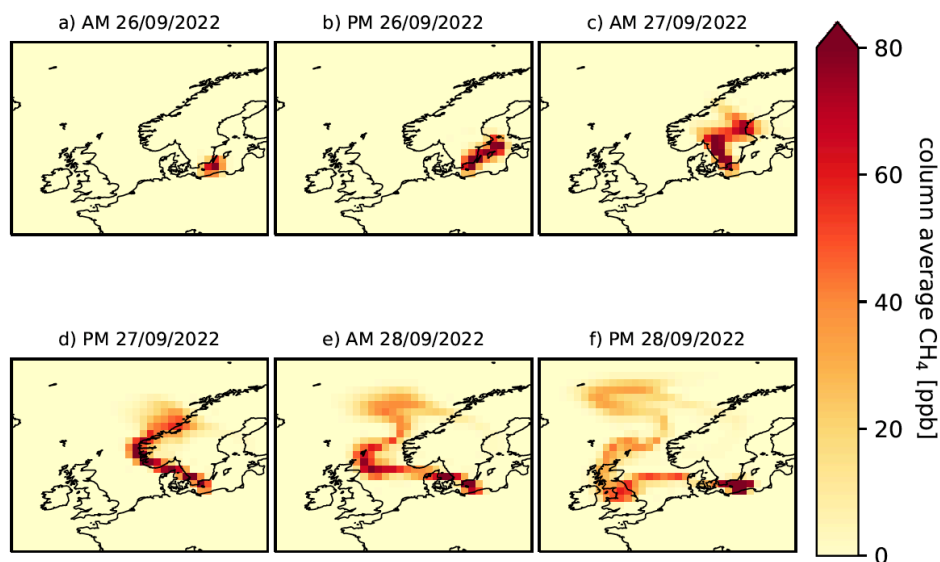


709

710 Figure 3: Observed (black line) and simulated (grey lines/coloured shading) CH₄ mixing ratios (ppb) at Integrated
711 Carbon Observation System (ICOS) sites during 26th – 29th September 2022. Observations and model output are both
712 averaged into hourly means. ICOS sites are at Birkenes, Norway (BIR), Norunda, Sweden (NOR), Hyltemossa,
713 Sweden (HTM) and Utö, Finland (UTO). See main text and Figure 1 for further details. Grey lines show TOMCAT-
714 simulated CH₄ using the two prior emission estimates, and shaded regions show the simulated min/max range for the
715 inversions with constant prior (blue) and decaying prior (red) optimised against individual retrievals, and for
716 inversions optimised against the regional mean (teal). Inlet heights are the highest available at each site: 75m at BIR;
717 100m at NOR; 150m at HTM and 57m at UTO. Note the different y-axis ranges in each panel.

718

719



720
721 Figure 4: Simulated TOMCAT column average CH₄ (ppb) from Nord Stream gas leaks for 26th–28th September
722 2022. Background CH₄ and emissions from sources other than Nord Stream are not included. Output times are
723 matched to IASI local overpass times, but IASI averaging kernels have not been applied. Column averages are
724 displayed on the model grid with horizontal resolution 1.125° × 1.125°. Emission rates from the leaks is constant at
725 4.17 Gg hr⁻¹, summing to 300 Gg in total over the three days.

726

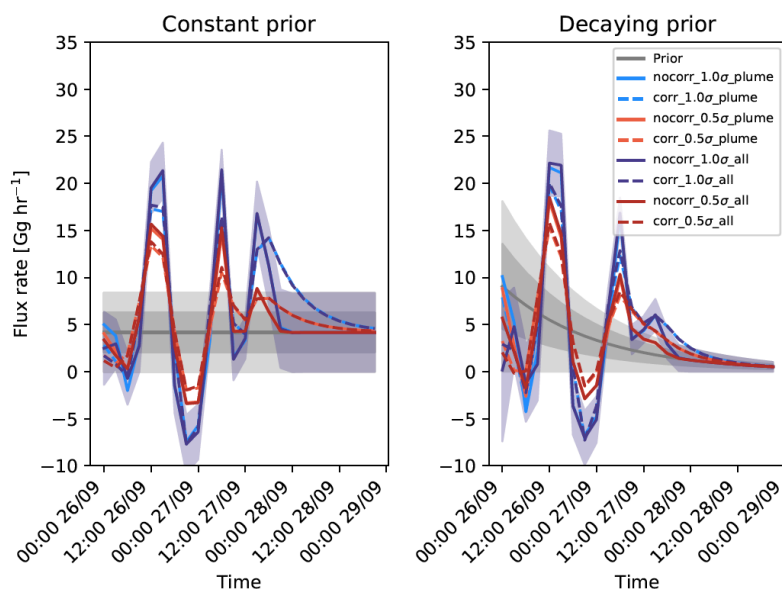
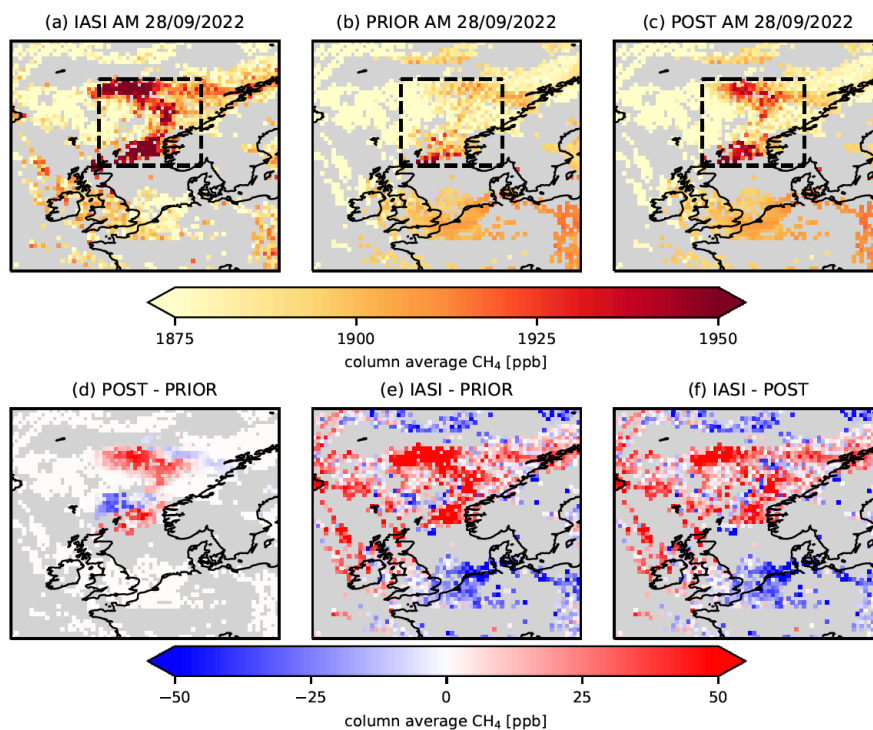


Figure 5: Prior and posterior CH_4 flux rates (Gg hr^{-1}) over the first three days (September 26th - 28th) of the Nord Stream leaks based on IASI data from the morning of 28th September 2022. Prior flux rate is shown in grey, with dark grey shaded region showing the 50% prior uncertainty and the light grey shaded region showing the 100% prior uncertainty. Dashed lines show posterior inversions with prior temporal correlations imposed; solid lines show those without prior correlations. Blue lines show inversions with 100% prior uncertainty imposed; red lines show those with 50% prior uncertainty. Darker shades show inversions based on all available IASI data; lighter shades show inversions based only on IASI data from near the plume, in the region highlighted in Figure 6. Shaded blue region shows the posterior uncertainty for the ‘nocorr_1.0σ_all’ case.

727
728
729
730
731
732
733
734
735
736



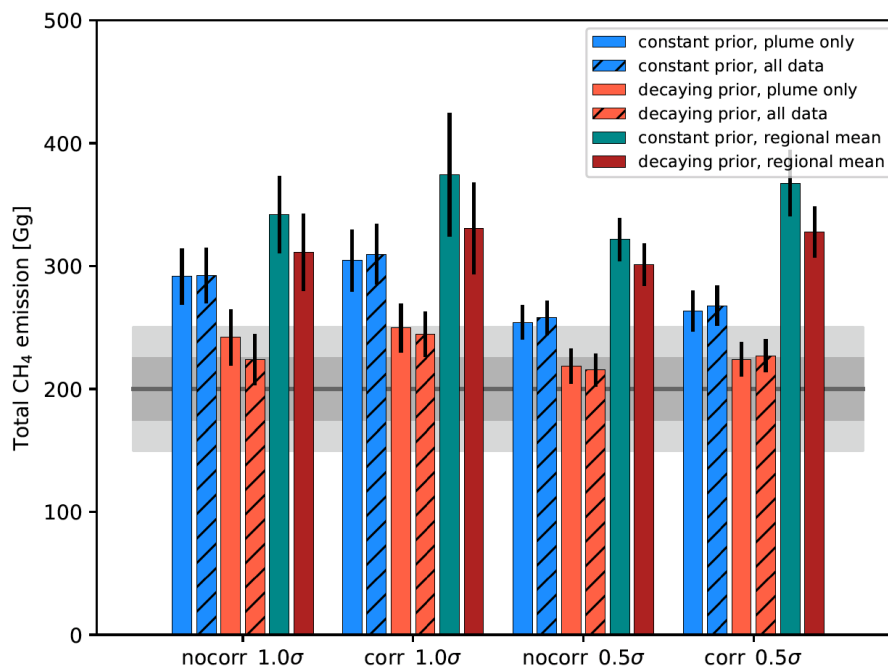
737
738
739
740
741
742
743
744

Figure 6: Column average CH₄ (ppb) on the morning of 28th September over the region of the Nord Stream gas leaks from (a) IASI; (b) TOMCAT using the constant prior emissions; and (c) TOMCAT using the nocorr_1.0_plume posterior emissions based on that prior. Also shown is the difference between the model posterior and prior (d); the difference between IASI and the model prior (e); and the difference between IASI and the model posterior (f). Retrievals and model output are averaged onto 0.25° × 0.25° grid boxes, weighted inversely to the observations' uncertainties. IASI averaging kernels are applied to the TOMCAT output. Black dashed line shows the 'plume' region defined in the text, used for optimising only the regional mean XCH₄ value.

745
746
747
748



749



750

751

752

753

754

755

756

757

758

759

760

Figure 7: Total (two-day) posterior CH₄ emissions (Gg) from the Nord Stream leaks during 26th – 27th September based on multiple different IASI-based inverse modelling calculations. Blue bars represent inversions with the constant prior where the model is optimised against individual IASI retrievals, whilst orange bars are the same but for the decaying prior. Turquoise bars represent inversions with the constant prior where the model is optimised against the mean XCH₄ in the plume region, whereas red bars are the same but for the decaying prior. Hatched bars show inversions in which all IASI data is included, and unhatched bars show inversions in which retrievals only within the plume region are included. ‘Corr’ and ‘nocorr’ refers to inversions with and without prior temporal correlations included, whilst 1σ and 0.5σ refer to inversions with 100% and 50% prior uncertainty. The grey solid line shows the prior emission total, with 50% and 100% 3-hour prior uncertainty shaded in dark and light grey, respectively.

761